Available online at www.sciencedirect.com
SCIENCE DIRECT®
Journal of Catalysis 221 (2004) 455–465
JOURNAL OF CATALYSIS
www.elsevier.com/locate/jcat

Influence of the support on the preferential oxidation of CO in hydrogen-rich steam reformates over the $CuO–CeO_2–ZrO_2$ system

P. Ratnasamy,* D. Srinivas, C.V.V. Satyanarayana, P. Manikandan, R.S. Senthil Kumaran, M. Sachin, and Vasudev N. Shetti

National Chemical Laboratory, Pune 411 008, India

Received 6 May 2003; revised 26 August 2003; accepted 2 September 2003

Abstract

Preferential oxidation (PROX) of CO in hydrogen-rich steam reformates was investigated using $CuO–CeO_2$, $CuO–CeO_2–ZrO_2$, and $CuO–ZrO_2$ catalysts. CuO (1–10 wt%) samples supported over high-surface-area ($S_{BET} = 117–172\ m^2/g$), cubic CeO_2, $CeO_2–ZrO_2$, and ZrO_2 were synthesized by coprecipitation. The composition of the support markedly influenced the PROX activity. Both $CuO–CeO_2$ and $CuO–CeO_2–ZrO_2$ exhibited higher activity and selectivity in CO oxidation than $CuO–ZrO_2$. The adverse influence of H_2O was accentuated in catalysts containing ZrO_2. Below 423 K and over $CuO–CeO_2$ with less than 5 wt% CuO, the presence of H_2O in the feed suppressed CO oxidation. H_2O had a negligible effect on H_2 oxidation. The catalysts showed stable activity in long-term experiments with the realistic feeds. The catalysts were characterized by XRD, surface area, TPR, diffuse reflectance UV–visible, EPR, and magnetic-susceptibility techniques. While a small amount of copper might be incorporated in the CeO_2/ZrO_2 fluorite lattice (forming a solid solution), most of it was at the surface of the support as isolated monomeric (types I and II) and dimeric (type IV) copper oxo species, nano-sized copper clusters containing magnetically interacting copper ions (type III) and a CuO-like, bulk phase. While the isolated copper oxo species exhibited reversible reduction–oxidation behavior, the interacting copper and CuO-like phases exhibited irreversible reduction behavior. The amount and reducibility of CuO on different supports correlated with their CO oxidation activities and increased in the order $CuO–ZrO_2 \leqslant CuO–CeO_2–ZrO_2 < CuO–CeO_2$.

Keywords: Preferential CO oxidation (PROX); PEM fuel cells; Supported CuO catalysts; $CuO–CeO_2$; $CuO–CeO_2–ZrO_2$; $CuO–ZrO_2$; Influence of support

1. Introduction

Selective CO removal from streams containing an excess of H_2 and significant amounts of CO_2 and H_2O is a current challenge in heterogeneous catalysis research especially in the preparation of H_2 suitable for polymer electrolyte membrane fuel cells (PEMFC) [1,2]. Hydrogen is usually generated from hydrocarbons or alcohols by steam/autothermal reforming followed by the water–gas shift (WGS) reaction [3]. Typical effluents from such a process contain about 0.3–1.0% of CO in a large excess of H_2 (40–75%) and about 20–25% CO_2. CO levels, however, have to be reduced to below 100 and, preferably, below 10 ppm for use in PEMFC [1]. Methanation, after removal of CO_2 by pressure swing adsorption, the conventional strategy used for CO removal in NH_3 or H_2 chemical plants, is impractical in the fuel cell context, especially for "on-board" use in vehicles. Preferential oxidation of CO to CO_2 without simultaneously oxidizing H_2 to H_2O (PROX) is one of the solutions. However, the latter oxidation is more exothermic and, hence, favored at high temperatures. Selective catalysts active at low temperatures are needed. Supported Pt [4,5], Rh [6], Pd [7], and Au [8] as well as base metal catalysts like CoO [9] and $CuO–CeO_2$ [10,11] have been investigated.

The PROX reaction has been extensively investigated [12–20]. However, in many of the studies reported so far, especially in the journal literature, the PROX reactor feed did not include CO_2, CH_4, or H_2O which occur in significant concentrations in the effluents from real-life reforming-cum-WGS processes and whose presence can lead to results not anticipated from studies with only a mixture of CO, O_2, and H_2. CH_4, for example, can be oxidized to CO/CO_2 under PROX conditions, especially over noble metal catalysts, and

* Corresponding author.
E-mail address: prs@ems.ncl.res.in (P. Ratnasamy).

0021-9517/$ – see front matter
doi:10.1016/j.jcat.2003.09.006

thereby lead to higher CO levels in the PROX reactor effluent. Again, in our laboratory, we had found that some of the reported catalysts, especially those based on Au, which were very active at very low temperatures (even below 373 K) exhibited activity decay in long-term studies, probably due to the strong adsorption of CO_2 (an "acid gas") and H_2O on some of the basic oxides used as supports for Au. On Pt–Al_2O_3, Korotkikh and Farrauto [21] reported that CO_2 does not affect CO oxidation; H_2O, however, decreased CO oxidation by about 10%. Such studies have not been reported for base metal PROX catalysis.

We now report an investigation of the preferential oxidation of CO over the CuO–CeO_2–ZrO_2 catalyst system using a feed composition more representative of the feed to a PROX reactor in a PEM fuel cell. CuO–CeO_2 exhibits significant activity in the total oxidation of CO [10]. The well-known enhancement of the total oxidation activity of CuO when supported on oxides like CeO_2 was attributed to a "synergistic" effect [11,22]. It is also known that addition of ZrO_2 (to form CeO_2–ZrO_2 solid solution) improves the oxygen-storage capacity of ceria and, in addition, retards the growth of CeO_2 crystallites [23]. Even though a large amount of structural studies on the CuO-CeO_2–ZrO_2 system has been carried out [24–29], the influence of the crystallite and particle size of cerium and zirconium oxides on the dispersion, oxidation states, magnetic properties, and catalytic activity, in PROX reactions, of copper catalysts supported on the CeO_2–ZrO_2 support is not understood completely. For example, what is the effect of varying the dispersion of ceria and CuO on the selectivity for oxidation of CO (vis-à-vis H_2 and CH_4) in the presence of CO_2 and H_2O? We have prepared samples of CuO–CeO_2–ZrO_2 with varying concentrations of the individual components and characterized their physicochemical properties by techniques such as XRD, temperature-programmed reduction, UV–visible and electron spin resonance spectroscopies, and magnetic susceptibility. The catalytic activity of these well-characterized samples in the selective oxidation of CO in a gas mixture with a composition similar to that present in typical PROX reactor effluents is also reported. The results enable us to throw further light on the influence of the structural characteristics of supported copper in these systems on their catalytic activity and selectivity in PROX reactions.

2. Experimental

2.1. Materials and catalyst preparation

$Ce(NO_3)_3 \cdot 6H_2O$ (SEMCO, Mumbai; 99.9%), $ZrO(NO_3)_2 \cdot xH_2O$ and $Cu(NO_3)_2 \cdot 3H_2O$ (LOBA Chemie, Mumbai; 99%) were used as sources of CeO_2, ZrO_2, and CuO, respectively.

2.1.1. Preparation of CuO–CeO_2 catalysts

In the preparation of CuO (1 wt%)—CeO_2 (99 wt%), 12.48 g of $Ce(NO_3)_3 \cdot 6H_2O$ was dissolved in 288 ml of distilled water and 0.152 g of $Cu(NO_3)_2 \cdot 3H_2O$ was dissolved in 6.3 ml of distilled water. These solutions were mixed together and added dropwise to a continuously stirred solution of KOH (0.1 M) taken in a 2 liter round bottom flask, placed in a heating mantle, and fitted with a pH electrode, water-cooled condenser and burette containing additional 0.1 M KOH solution. During addition, the temperature of the flask was maintained at 353 K and pH 10. The cations were precipitated in the form of their hydroxides. The mixture was digested at 353 K for 3 h and then cooled to 298 K. The precipitate was separated and washed copiously with distilled water until all the potassium ions were removed. It was then dried in an air oven, at 393 K, for 8 h. Later the dried material was crushed into powder and calcined in air, at 773 K, for 5 h, to get the final product. It may be noted that potassium is an effective element for preferential oxidation of CO in a H_2-rich stream [30]. Absence of potassium ions in the final product was determined by atomic absorption spectroscopy (AAS, Varian Spectr SF-220).

2.1.2. Preparation of CuO–ZrO_2 catalysts

The CuO–ZrO_2 catalysts were prepared in a similar manner as described above. In a typical preparation of CuO (1 wt%)–ZrO_2 (99 wt%) (5 g batch), 9.28 g of $ZrO(NO_3)_2 \cdot xH_2O$ dissolved in 400 ml distilled water and 0.152 g of $Cu(NO_3)_2 \cdot 3H_2O$ dissolved in 6.3 ml distilled water were used.

2.1.3. Preparation of CuO–CeO_2–ZrO_2 catalysts

The Ce:Zr ratio in these catalysts is 1:1 wt%. In the preparation of CuO (1 wt%)–CeO_2 (49.5 wt%)–ZrO_2 (49.5 wt%) (5 g batch), 6.24 g of $Ce(NO_3)_3 \cdot 6H_2O$ dissolved in 144 ml of distilled water, 4.64 g of $ZrO(NO_3)_2 \cdot xH_2O$ dissolved in 200 ml of distilled water, and 0.152 g of $Cu(NO_3)_2 \cdot 3H_2O$ dissolved in 6.3 ml of distilled water were used. The catalysts were prepared in a similar manner as described above.

For comparison, pure ceria, zirconia and ceria-zirconia (1:1 wt%) samples were also prepared.

2.2. Catalyst characterization

A Rigaku Geigerflex X-ray diffractometer with Ni-filtered Cu-K_α radiation ($\lambda = 1.5406$ Å, 40 kV, 30 mA) was used to determine the crystallinity and phase purity of the samples. The XRD patterns were recorded in the 2θ range of 20–90°, with a scan speed of 2°/min. The average crystallite size was determined from the linewidths of the XRD peaks corresponding to (111) reflection, using the Debye–Scherrer equation. The specific surface area (S_{BET}) was estimated from the N_2 adsorption/desorption isotherms, measured at 77 K, using a Coulter 100 instrument.

Temperature-programmed reduction (TPR) experiments were performed using a Micromeritics AutoChem 2910 in-

strument. A weighed amount (20 mg) of the sample was placed in a quartz reactor and treated with a O_2 (22%)–He (78%) gas mixture at 773 K for 2 h. A gas mixture of H_2 (5%)–Ar (95%) was then passed (30.22 ml/min) through the reactor. The temperature was raised to 1200 K at a heating rate of 10 K/min. A standard CuO powder was used to calibrate the amount of H_2 consumption.

Diffuse reflectance UV–visible (DRUV–visible) spectra were recorded on a Shimadzu UV-2550 spectrophotometer equipped with an integrating sphere attachment (ISR-2200). Spectral grade $BaSO_4$ was the reference material. In situ EPR measurements were done on a Bruker EMX spectrometer operating at X-band frequency ($\nu \approx 9.4$ GHz) and 100-kHz field modulation. The calcined sample (40 mg) was taken in a specially designed quartz EPR cell (o.d. = 4 mm) fitted with greaseless stopcocks and provision for adsorption/desorption of gases. Prior to EPR measurements, the samples were degassed at 773 K for 6 h (10^{-3} Torr) and then treated with dry hydrogen (20 ml/h) for 1 h at elevated temperatures. The spectra were recorded at both 298 and 77 K. No marked changes in spectral resolution were observed at lower temperatures.

Magnetic susceptibility measurements at 298 K (10–15 mg catalyst) were carried out with a Lewis-coil force magnetometer (Series 300, George Associates, USA) coupled with a high-vacuum system (10^{-6} Torr) with provision for in situ treatment in desired gases at elevated temperatures. Corrections for sample holder and ferromagnetic impurities, if any, were also made.

2.3. Catalytic activity studies

PROX reactions were carried out in a fixed bed, downflow, glass reactor (i.d. = 15 mm) using 1.5 g of the calcined catalyst. The sample was made into a pellet (without any binder), crushed, and sized (10–20 mesh). Then, it was activated at 573 K, for 3 h, in flowing hydrogen and then cooled to 403–473 K. A synthetic feed gas mixture of volume composition H_2 (74.17%) + CO (0.49%) + CO_2 (23.26%) + CH_4 (2.08%) was passed through a mass flow controller at a specified flow rate (2.5–10 liters/h; GHSV = 5000–20,000h^{-1}) along with the required amount of oxygen in air (O_2/CO = 0.5–1.5). Experiments were also conducted with a stream containing added water (1.25 ml/h; $p(H_2O) = 200$ Torr) or an actual effluent from a steam reformer-cum-water–gas-shift reactor processing LPG was passed directly (after addition of oxygen) into the PROX reactor. The products were analyzed online using a CHEMITO 8610 gas chromatograph equipped with a methanator. A Spherocarb column (1/8 inch diameter × 8 feet length) was used for analysis. A calibrated gas was used as a reference to estimate the concentrations of gases.

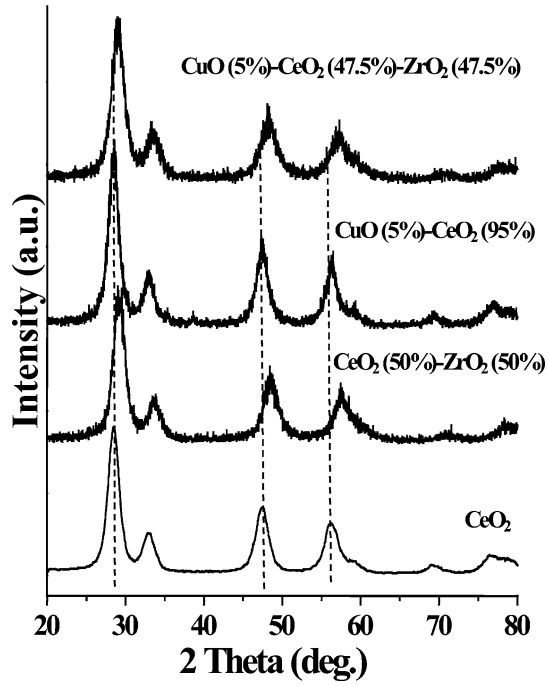

Fig. 1. XRD profiles of CuO–CeO_2–ZrO_2 samples.

3. Results and discussion

3.1. Structural and textural studies

Fig. 1 shows the XRD patterns of CeO_2, CeO_2 (50%)–ZrO_2 (50%), CuO (5%)–CeO_2 (95%), and CuO (5%)–CeO_2 (47.5%)–ZrO_2 (47.5%). The reflections in the 2θ range of 28–80° indicate a distinct, cubic, fluorite structure [24–29]. In CeO_2–ZrO_2-based catalysts the reflections shifted to higher 2θ values compared to CeO_2 (shown by dotted lines in Fig. 1). The unit cell parameter (Table 1) of CeO_2–ZrO_2 is smaller (0.531 nm) than that of CeO_2 (0.548 nm), suggesting the formation of ceria–zirconia solid solutions [31]. The ZrO_2-based catalysts showed broad reflections and hence, the unit cell and average crystallite size parameters could not be determined with precision. No separate phase due to CuO or Cu_2O was detected, except in the samples with 10 wt% CuO. A majority of the total CuO is present at the surface of the support.

The presence of zirconium decreased the crystallite size of ceria as well as CuO (Table 1). The crystallite size of ceria decreased from 8.4 (for CuO (10%)–CeO_2 (90%)) to 3.8 nm (for CuO (10%)–CeO_2 (45%)–ZrO_2 (45%)). The corresponding decrease in the crystallite size of CuO was from 4.1 to 3.2 nm. When CuO was also present the crystallite size of ceria increased from 4.9 nm (for pure CeO_2) to 8.4 nm (for CuO (10%)–CeO_2 (90%)).

S_{BET} values increased in the series: CeO_2 < CeO_2–ZrO_2 < ZrO_2 (Table 1). When CuO was also present, the CuO–CeO_2 samples showed a marked decrease in surface area (from 150 to 117 m^2/g). The decrease is not significant in CuO–CeO_2–ZrO_2 (Table 1). Zirconia incorporation in the

Table 1
Structural parameters (from XRD) and BET surface areas of CuO-CeO_2–ZrO_2 composites

Catalyst[a]	Unit cell parameter of the support oxide (nm)	Average crystallite size of the support oxide (nm)	Unit cell parameter of CuO (nm)	Average crystallite size of CuO (nm)	S_{BET} (m^2/g)
CeO_2	0.548	4.9	–	–	150
CeO_2 (50%)–ZrO_2 (50%)	0.531	4.4	–	–	161
ZrO_2	–	–	–	–	172
CuO (1%)–CeO_2 (99%)	0.547	6.6	–	–	117
CuO (5%)–CeO_2 (95%)	0.545	7.8	–	–	129
CuO (10%)–CeO_2 (90%)	0.542	8.4	0.438	4.1	124
CuO (1%)–CeO_2 (49.5%)–ZrO_2 (49.5%)	0.532	4.4	–	–	168
CuO (5%)–CeO_2 (47.5%)–ZrO_2 (47.5%)	0.533	4.2	–	–	148
CuO (10%)–CeO_2 (45%)–ZrO_2 (45%)	0.530	3.8	0.437	3.2	136
CuO (1%)–ZrO_2 (99%)[b]	–	–	–	–	161
CuO (5%)–ZrO_2 (95%)[b]	–	–	–	–	153
CuO (10%)–ZrO_2 (90%)[b]	–	–	–	–	161

[a] Values in parentheses indicate composition in wt%.
[b] XRD peaks were broad.

support, hence, increases the surface area of the samples in agreement with the XRD results where formation of smaller crystallites is found in CeO_2–ZrO_2-based catalysts (Table 1; compare rows 7–9 with 4–6).

3.2. Redox behavior, spectral and magnetic properties

3.2.1. Temperature-programmed reduction

Pure ZrO_2 could not be reduced in H_2 in the temperature range 298–1200 K. CeO_2 showed two peaks at 658 and 794 K attributable to the reduction of surface and bulk ceria compositions, respectively [23,28]. In the presence of zirconia the reducibility of ceria increased and the reduction temperature decreased. In CeO_2–ZrO_2, the reduction of surface and bulk ceria occurred at 620 and 804 K, respectively.

Reduction of CuO supported on CeO_2, CeO_2–ZrO_2 and ZrO_2 started above 373 K [28,29]. In pure CuO this occurred above 523 K. At least 2 to 3 reduction peaks were observed in the supported catalysts, indicating the existence of different type of CuO species. CuO (5%)–ZrO_2 (95%) showed overlapping reduction peaks at 465 K and 450 K (Fig. 2). These peaks in CuO (5%)–CeO_2 (95%) appeared at lower temperatures, 445 and 425 K, respectively (Fig. 2). In CuO (5%)–CeO_2 (47.5%)–ZrO_2 (47.5%), they occurred at still lower temperatures, 435 and 398 K, respectively (Fig. 2). With different supports, the reducibility of CuO increased in the order $ZrO_2 < CeO_2 < CeO_2$–ZrO_2. TPR of CuO supported on CeO_2 and ZrO_2 was investigated by several groups [32–34]. They observed CuO reduction peaks in the range 398–448 K and above 473 K. The former was attributed to arise from dispersed copper oxide clusters, strongly interacting with the support while the latter (above 473 K) from CuO particles. The TPR peaks for our catalysts (Fig. 2) reveal that the latter type of CuO particles is not present in our catalyst samples and the CuO is mostly well dispersed.

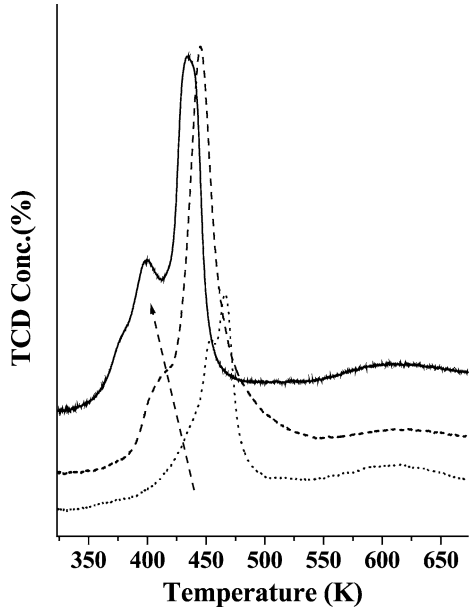

Fig. 2. TPR of CuO (5%)–ZrO_2 (95%) (···), CuO (5%)–CeO_2 (95%) (- - -), and CuO (5%)–CeO_2 (47.5%)–ZrO_2 (47.5%) (—).

3.2.2. Electronic spectroscopy

Both pure CeO_2 and CeO_2–ZrO_2 showed two UV bands at 257 and 338 nm attributable to $O^{2-} \rightarrow Ce^{4+}$ charge transfer (CT) transitions. The former is a specular reflectance band arising from the surface sites and the latter is a diffuse reflectance band arising from bulk ceria [35]. Pure ZrO_2 showed only one band at 215 nm. The extinction coefficients of these bands were different for different supports and decreased in the order $CeO_2 > CeO_2$–$ZrO_2 > ZrO_2$. The intensity of the 338-nm band in CeO_2–ZrO_2 (vis-à-vis pure CeO_2) increased due to the substitution of Zr^{4+} in the CeO_2 lattice and the consequent strain and lowering of symmetry at the site of cerium. These CT bands shifted to the lower energy side (higher wavelength) when CuO was

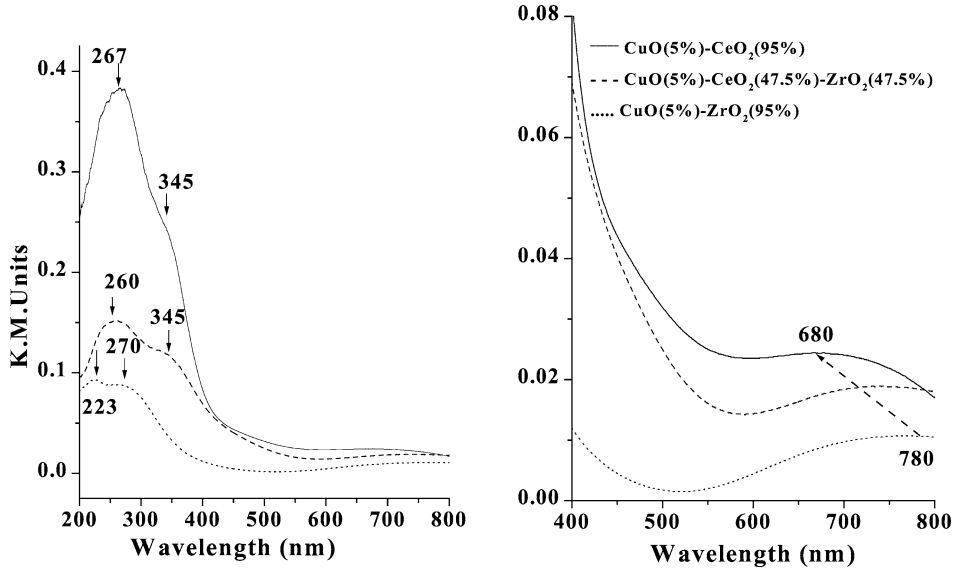

Fig. 3. DRUV–visible spectra showing the influence of support composition on the charge transfer (left) and *d–d* (right) transitions.

also present (Fig. 3, left panel). The shift is more noticeable in CuO–CeO_2 and CuO–ZrO_2 than in CuO–CeO_2–ZrO_2. In CuO (5%)–CeO_2 (95%), these CT appeared at 267 and 345 nm (compared to 257 and 338 nm, respectively). In CuO (5%)–CeO_2 (47.5%)–ZrO_2 (47.5%), they appeared at 260 and 345 nm. In CuO (5%)–ZrO_2 (95%), the 215-nm band shifted to 270 nm. These red shifts in the CT bands reveal an increase in the crystallite size of CeO_2 in the presence of CuO. These observations reinforce similar conclusions from the XRD data (Table 1).

The CuO-containing catalysts showed a broad, *d–d* band in the visible region (Fig. 3, right panel). This band shifted from 780 (Cu^{2+} in sixfold coordination) to 680 nm (Cu^{2+} in fourfold coordination) with a change in the support from ZrO_2 to CeO_2–ZrO_2 to CeO_2, respectively [36–38]. A similar shift (from 800 to 763 nm in CuO–ZrO_2, 768 to 645 nm in CuO–CeO_2–ZrO_2, and 670 to 650 nm in CuO–CeO_2) was observed with an increase (from 1 to 10 wt%) in the CuO content, indicating that the type of copper species in these catalysts is influenced by both the support and the concentration.

3.2.3. EPR spectroscopy

3.2.3.1. Redox behavior of the support EPR spectra of CeO_2 reduced with dry hydrogen revealed the formation of two types of paramagnetic species, A, due to Ce^{3+} [39] ($g_\perp = 1.965$ and $g_\parallel = 1.940$) and B, due to $O_2^{-\cdot}$ ions [40] ($g_1 = 2.030$, $g_2 = 2.016$, and $g_3 = 2.011$), the concentration of which depended on the reduction temperature (T_r) (Fig. 4, left panel). Intensity of *A* signals reached a maximum at 573 K. Pure ZrO_2 did not form these paramagnetic species when reduced in hydrogen. CeO_2–ZrO_2 (Fig. 4, right panel) behaved in a manner similar to pure CeO_2. Upon reoxidation by exposure to air at 298 K, the signals due to species A disappeared and of B decreased and broadened.

Species A and B could be generated, repeatedly, in several cycles, indicating the facile redox behavior of CeO_2 and CeO_2–ZrO_2 supports. TPR had indicated that the reduction of ceria (not shown in figure) is facilitated in the presence of zirconia. The reduction of ceria occurred at 620 K in CeO_2–ZrO_2 compared to 658 K in CeO_2. Hence, higher amounts of Ce^{3+} are formed in reduced CeO_2–ZrO_2 composites than in pure CeO_2. Both EPR and TPR studies reveal that zirconium incorporation enhances the concentration of Ce^{3+}.

3.2.3.2. Redox behavior of supported copper At least four types of paramagnetic copper species (I–IV) could be identified in the EPR spectrum of CuO (1%)–CeO_2 (99%) (Fig. 5i, curve a). Types I and II correspond to isolated, monomeric Cu^{2+} species characterized by axial spectra with resolved Cu hyperfine features in the parallel and perpendicular regions [24–26,41,42]. These species are different in their $g_\parallel$ and $A_\parallel$(Cu) values (type 1: $g_\parallel = 2.300$, $A_\parallel(\mathrm{Cu}) = 126.4$ G; type 2: $g_\parallel = 2.339$, $A_\parallel(\mathrm{Cu}) = 124.8$ G). Their $g_\perp(2.049)$ and $A_\perp$(Cu) (10.0 G) values are similar. The linewidth of species I is smaller than that of species II (curve a). The spin Hamiltonian parameters indicate that the geometry around Cu^{2+} is distorted octahedral. These species (I and II) are perhaps located in the lattice and surface sites of ceria crystallites, respectively [41]. The type III species characterized by a broad signal (linewidth = 210 G) centered at $g_{av} = 2.10$ is attributed to dipolar, interacting Cu^{2+} ions forming a nano-sized 2-dimensional structure [41]. The relative concentration of the type III species increased with copper content (Fig. 5ii). The visible band at 645–680 nm in the diffuse reflectance spectrum corresponds to this species. The type IV species showed two signals at 3017 and 3716 G corresponding to a single-quantum, perpendicular transitions of Cu^{2+}–Cu^{2+} dimers at the surface [42]. The exchange coupling constant (J) for these dimers (type IV) was -52.5 cm^{-1} and the Cu–Cu separa-

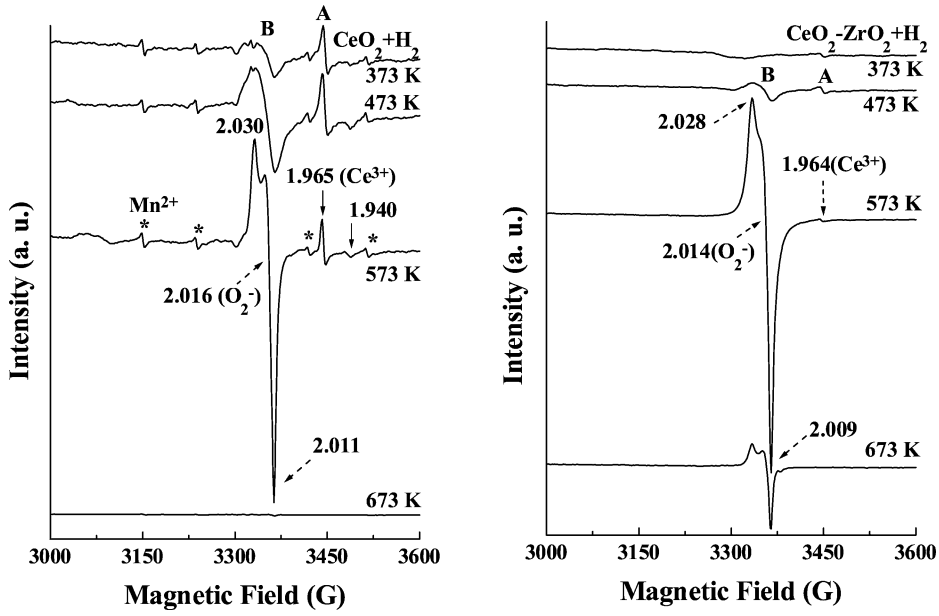

Fig. 4. EPR spectra (at 298 K) of Ce^{3+} (A) and $O_2^{-\bullet}$ (B) ions generated on CeO_2 (left) and CeO_2–ZrO_2 (right) by reaction with H_2 at elevated temperatures.

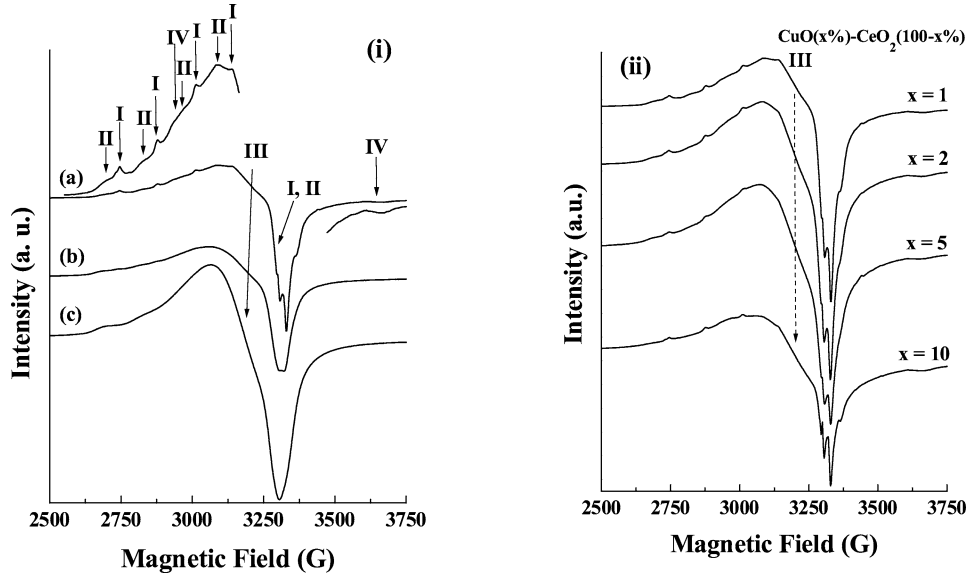

Fig. 5. (Left) EPR spectra of CuO (1%) supported on (a) CeO_2, (b) CeO_2–ZrO_2, and (c) ZrO_2. Signals due to different Cu species (I, II, III, and IV) are indicated by arrows. (Right) Effect of CuO content on the EPR spectra of CuO (x%)–CeO_2 ((100 − x)%) catalysts.

tion was 3.4 Å [42]. If the two copper ions of the dimer were to occupy adjacent Ce^{4+} locations in the fluorite lattice, their Cu–Cu separation would have been 5.41 Å. It was, hence, proposed that these interacting, Cu^{2+}–Cu^{2+} dimers in copper oxo species are at the surface of ceria [41,42].

CuO (1%)–ZrO_2 (99%), on the other hand, contained only two types of Cu^{2+} species, viz. isolated Cu^{2+} ions (II) and interacting Cu^{2+} ions (III) (Fig. 5i, curve c). The spin Hamiltonian parameters of these species are different from CuO (1%)–CeO_2 (99%) (Table 2). Unlike in CuO (1%)–CeO_2 (99%) (Fig. 5i, curve a), the perpendicular Cu-hyperfine features could not be resolved in CuO (1%)–ZrO_2 (99%) (Fig. 5i, curve c). The type III species of CuO–ZrO_2 showed a signal at $g_{av} = 2.12$.

CuO (1%)–CeO_2 (49.5%)–ZrO_2 (49.5%) showed spectra (Fig. 5i, curve b) intermediate in shape to that of CuO (1%)–CeO_2 (99%) and CuO (1%)–ZrO_2 (99%). Cu species, types I, II, and III were detected. Similar to CuO (1%)–CeO_2 (99%), the type I species of CuO (1%)–CeO_2 (49.5%)–ZrO_2 (49.5%) showed resolved Cu-hyperfine features at parallel and perpendicular regions (Table 2). Signals of CuO (1%)–CeO_2 (49.5%)–ZrO_2 (49.5%) were broader. Cu^{2+}–Cu^{2+} dimers (type IV) could not be detected. Thus, different types of CuO species were present in different amounts on CeO_2, ZrO_2, and CeO_2–ZrO_2.

Table 2
EPR spin Hamiltonian parameters

Catalyst	Treatment	Assignment	Type	$g_\parallel$ or g_1	$g_\perp$ or g_2, g_3	$A_\parallel$(Cu) (G)	$A_\perp$(Cu) (G)
CeO_2	H_2 reduction	Ce^{3+}	A	1.940	1.965	–	–
		Ce^{4+}–$O_2^{-\cdot}$	B	2.030	2.011, 2.016	–	–
CeO_2 (50%)–ZrO_2 (50%)	H_2 reduction	Ce^{3+}	A	1.940	1.964	–	–
		Ce^{4+}–$O_2^{-\cdot}$	B	2.028	2.009, 2.014	–	–
CuO (1%)–CeO_2 (99%)	–	Isolated Cu^{2+} in lattice site	I	2.300	2.049	126.4	10
	–	Isolated surface Cu^{2+}	II	2.339	2.049	124.8	Not resolved
		Interacting Cu^{2+}	III	2.10	2.10	Not resolved	Not resolved
		Isolated dimer	IV[a]				
CuO (1%)–ZrO_2 (99%)		Isolated surface Cu^{2+}	II	2.336	2.063	130.0	Not resolved
		Interacting Cu^{2+}	III	2.12	2.12	Not resolved	Not resolved
CuO (1%)–CeO_2 (49.5%)–	–	Isolated Cu^{2+} in lattice site	I	2.300	2.060	126.4	10
ZrO_2 (49.5%)	–	Isolated surface Cu^{2+}	II	2.339	2.060	124.8	Not resolved
		Interacting Cu^{2+}	III	2.13	2.13	Not resolved	Not resolved

[a] $g_\perp$ signals due to type IV were observed at 3017 and 3716 G; $g_\parallel$ signals were weak and masked by types I–III.

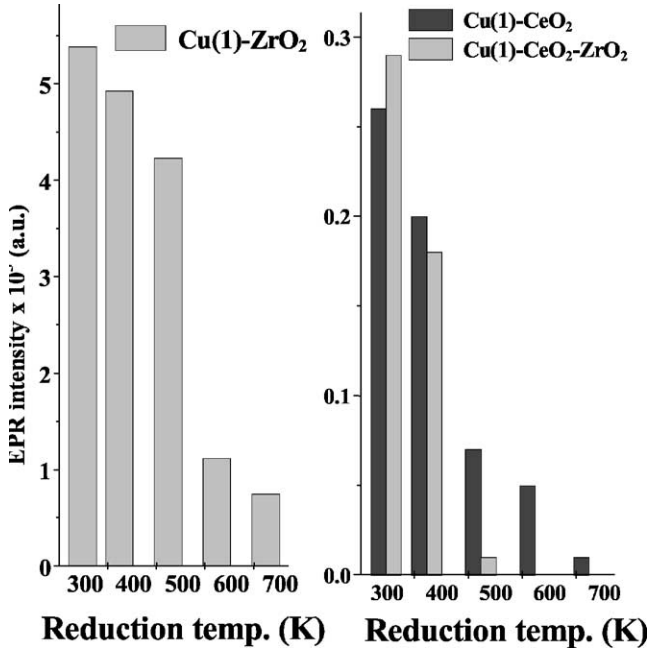

Fig. 6. Variation of Cu^{2+} signal intensity of CuO (1%)–CeO_2 (99%), CuO (1%)–CeO_2 (49.5%)–ZrO_2 (49.5%), and CuO (1%)–ZrO_2 (99%) as a function of reduction temperature.

The reducibility of CuO on various supports increased in the order CuO–ZrO_2 < CuO–CeO_2 < CuO–CeO_2–ZrO_2 (Fig. 6). When Cu–CeO_2 and Cu–CeO_2–ZrO_2 were reduced at 573 K, almost all the copper was reduced. Reoxidation by exposing the samples to air regenerated the EPR spectrum of types I, II, and IV species. Type III species could not be regenerated. The reduction–reoxidation of types I, II, and IV species (isolated/dispersed copper) could be repeated several times. A similar observation was noted also on CeO_2–ZrO_2 supports. While 39.7% of total intensity could be regenerated upon reduction followed by reoxidation in CuO–CeO_2, it was only 31.4% in CuO–CeO_2–ZrO_2. Hence, the amount of reactive copper oxide that could be reduced and reoxidized is more on CeO_2 than on CeO_2–ZrO_2 support. The facile redox behavior and the abundance of the reactive copper species influence the CO oxidation activity of these catalysts (vide supra). In the absence of CuO, the supports CeO_2 and CeO_2–ZrO_2 generated Ce^{3+} ions and $O_2^{-\cdot}$ species. Such species were not detected in supported CuO catalysts.

3.2.4. Magnetic susceptibility

Prior to magnetic susceptibility measurements the samples were first evacuated and then purged with He (5–10 ml/h) and again evacuated. Molar susceptibilities (χ_M) of ZrO_2, CeO_2–ZrO_2, and CeO_2 after diamagnetic correction are 0.026×10^{-3}, 0.029×10^{-3}, and 0.060×10^{-3} c.g.s. units, respectively. These values indicate weak paramagnetism. The Mn impurity and paramagnetic ions like Ce^{3+} and defect centers generated by evacuation/dehydroxylation are the probable causes for the weak paramagnetism of the evacuated samples. The variation in magnetic susceptibility (χ_M) of the samples with increasing CuO content is shown in Fig. 7. The support influences the dispersion and magnetic state of copper significantly. From the linear increase in magnetic susceptibility, it may be concluded that the concentration of isolated, noninteracting Cu^{2+} ion increases with copper content in CeO_2–ZrO_2 (it may be recalled that Cu^{2+} is mainly responsible for the observed magnetic susceptibility). The presence of Cu^{1+} and *interacting* Cu^{2+} ions (at high concentrations) in CeO_2 and ZrO_2 probably account for their lower χ_M values at CuO content above 2 wt% (Fig. 7). In other words, in samples containing more than 2 wt% CuO, larger amounts of interacting Cu^{2+} ions/bulk CuO-like phases are formed on ZrO_2 and CeO_2 supports compared to CeO_2–ZrO_2. Apparently, CeO_2–ZrO_2 promotes a better and more stable dispersion of copper oxide. These results reinforce the conclusion from XRD (Table 1) that the average crystallite size of CuO on CeO_2–ZrO_2 is indeed smaller than that on CeO_2.

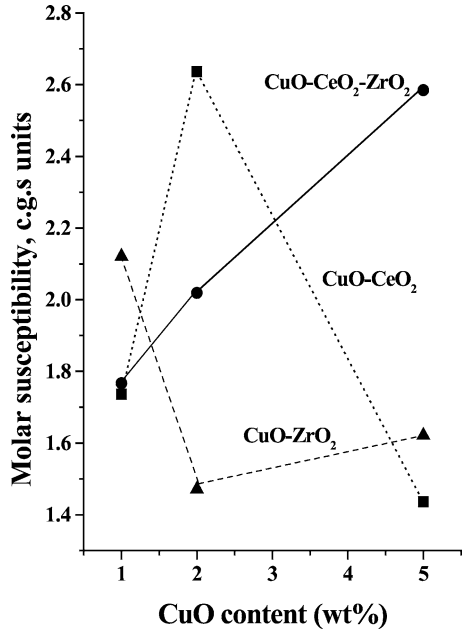

Fig. 7. Plot of molar magnetic susceptibility (χ_M) as a function of CuO content in CuO–CeO_2, CuO–CeO_2–ZrO_2, and CuO–ZrO_2.

3.3. Preferential oxidation of CO (PROX)

Catalytic activities of CuO supported on CeO_2, CeO_2–ZrO_2, and ZrO_2 under different reaction conditions (e.g., temperature, O_2/CO ratio, space velocity, and time on stream) are presented in Tables 3–5 and Figs. 8–10. PROX selectivity is defined as (oxygen consumed in CO oxidation) $\times 100$/(oxygen consumed in the oxidation of CO and H_2). Under our reaction conditions oxidation of CH_4 was not observed. Oxygen conversion was more than 99.8%. The following conclusions are drawn:

1. CO oxidation increased with CuO content reaching a maximum at 5 wt% (Table 3; rows 1–4). CuO supported on CeO_2 exhibited superior activity than CuO–CeO_2–ZrO_2 and CuO–ZrO_2 (Table 3; compare rows 3, 5 and 6).
2. With a water-containing feed ($p(H_2O) = 200$ Torr), a decrease in the CO oxidation activity was observed. This decrease is more significant with ZrO_2-containing catalysts (Table 3, rows 5 and 6) and in the catalysts with a lower CuO content (rows 1 and 2).
3. The adverse influence of H_2O on CO oxidation activity diminished above 423 K (Table 4).

Table 3
Preferential oxidation of CO over CuO–CeO_2–ZrO_2 catalysts

Catalyst	Feed without water					Feed with water[b]				
	CO		H_2		Selectivity[a]	CO		H_2		Selectivity[a]
	Composition ppm	Conversion (%)	Composition (v%)	Conversion (%)	(%)	Composition ppm	Conversion (%)	Composition (v%)	Conversion (%)	(%)
CuO (1%)–CeO_2 (99%)	98	98.0	73.4	1.0	38.4	3070	37.3	73.1	1.4	14.6
CuO (2%)–CeO_2 (98%)	82	98.3	73.4	1.0	38.5	1620	66.9	73.3	1.2	26.2
CuO (5%)–CeO_2 (95%)	7	99.9	73.4	1.0	39.1	17	99.7	73.4	1.0	39.0
CuO (10%)–CeO_2 (90%)	64	98.7	73.4	1.0	38.7	80	98.4	73.4	1.0	38.6
CuO (5%)–CeO_2 (47.5%)–ZrO_2 (47.5%)	89	98.2	73.4	1.0	38.5	495	89.9	73.4	1.0	35.2
CuO (5%)–ZrO_2 (95%)	2950	39.8	73.1	1.4	15.6	3500	28.6	73.1	1.5	11.2

Reaction conditions: catalyst = 1.5 g, feed, H_2 (74.17%) + CO (0.49%) + CO_2 (23.26%) + CH_4 (2.08%); O_2/CO = 1.25, GHSV = 5000 h^{-1}; temperature = 423 K; run time = 4 h.
[a] Selectivity of oxygen toward CO oxidation = (oxygen consumed in CO oxidation) $\times 100$/(total oxygen consumed in CO + H_2 oxidation).
[b] $p(H_2O) = 200$ Torr.

Table 4
Effect of temperature on the PROX activity over CuO (5%)–CeO_2 (47.5%)–ZrO_2 (47.5%)

Temperature (K)	Feed without water					Feed with water[b]				
	CO		H_2		Selectivity[a]	CO		H_2		Selectivity[a]
	Composition ppm	Conversion (%)	Composition (v%)	Conversion (%)	(%)	Composition ppm	Conversion (%)	Composition (v%)	Conversion (%)	(%)
373	2760	43.7	73.6	0.8	27.0	3610	26.3	73.6	0.8	18.5
398	775	84.1	73.5	0.9	38.1	2330	52.4	73.5	0.9	27.7
423	89	98.2	73.4	1.0	38.5	495	89.9	73.4	1.0	35.2
448	443	90.9	73.4	1.0	35.7	140	97.1	73.4	1.0	38.1
473	930	81.0	73.3	1.1	31.8	852	82.6	73.3	1.1	32.4

Reaction conditions: catalyst = 1.5 g, feed, H_2 (74.17%) + CO (0.49%) + CO_2 (23.26%) + CH_4 (2.08%); O_2/CO = 1.25, GHSV = 5000 h^{-1}.
[a] Selectivity of oxygen toward CO oxidation = (oxygen consumed in CO oxidation) $\times 100$/(total oxygen consumed in CO + H_2 oxidation).
[b] $p(H_2O) = 200$ Torr.

Table 5
Preferential oxidation of CO in the effluent from LTS on $CuO–CeO_2–ZrO_2$

Catalyst	Conversion of CO (%)	Conversion of H_2 (%)	Selectivity[a]
CuO (5%)–CeO_2 (95%)	99.95	2.8	20.3
CuO (5%)–CeO_2 (47.5%)–ZrO_2 (47.5%)	99.5	0.8	47.0
CuO (5%)–ZrO_2 (95%)	53.0	0.8	32.1

Reaction conditions: average feed composition, 5000 ppm CO + 20% CO_2 + 70% H_2 + balance H_2O + CH_4; GHSV = 20,000 h^{-1}, catalyst = 1.5 g, $O_2/CO = 1.25$; temperature = 423 K.
[a] Selectivity of oxygen toward CO oxidation = (oxygen consumed in CO oxidation) ×100/(total oxygen consumed in CO + H_2 oxidation).

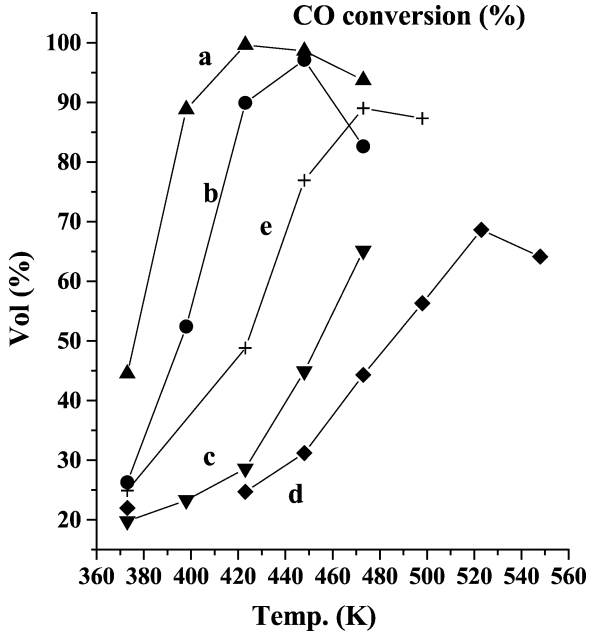

Fig. 8. Influence of support and temperature on the conversion of CO to CO_2. Reaction conditions: catalyst = 1.5 g; feed (H_2 (74.17%) + CO (0.49%) + CO_2 (23.26%) + CH_4 (2.08 v%)) + water ($p(H_2O) = 200$ Torr); $O_2/CO = 1.25$, GHSV = 5000 h^{-1}; run time = 4 h: (a) CuO (5%)–CeO_2 (47.5%)–ZrO_2 (47.5%); (b) CuO (5%)–CeO_2 (95%); (c) CuO (5%)–ZrO_2 (95%); (d) CeO_2; (e) CeO_2 (50%)–ZrO_2 (50%).

4. The CO oxidation activity/selectivity increased with temperature reaching a maximum at 448–478 K (Table 4) due either to increased H_2 oxidation at higher temperatures and/or to the growth of CuO particles above around 470 K [43].
5. The support has a marked effect on the catalytic activity (Fig. 8). With water-containing feed ($p(H_2O) =$ 200 Torr), the CO oxidation activity decreased in the order $CuO–CeO_2 > CuO–CeO_2–ZrO_2 > CuO–ZrO_2$. Copper-free supports also catalyzed the oxidation of CO and H_2. But their activities were considerably lower than the copper-containing catalysts. H_2 oxidation takes place on both the metal and the support.
6. $CuO–CeO_2$ and $CuO–CeO_2–ZrO_2$ samples exhibited a stable activity in long-term (18 h) experiments (Fig. 9).
7. At high space velocities, in the presence of water in the feed, while the H_2 conversion was not affected, the CO conversion and PROX selectivity were decreased (Fig. 10, left panel). As expected the PROX *selectivity* was high (94.9%) at a low value of O_2/CO.
8. CO oxidation increased with an increase in O_2/CO ratio. Almost complete conversion of CO to CO_2 was observed beyond a O_2/CO ratio of 1.25 (Fig. 10, right panel).
9. Table 5 illustrates the PROX activity for a feed consisting of the effluent from a fuel processor (steam reformer-cum-high temperature (HTS)-cum-low temperature water–gas-shift (LTS) reactors combination). Indian LPG (liquefied petroleum gas), comprising mostly C_3 and C_4 hydrocarbons (both saturates and olefins), was the feed to the steam reformer. 40% NiO–30% CeO_2–30% ZrO_2 was the steam-reforming catalyst operating at 923 K, GHSV = 20,000 h^{-1}, and steam/carbon = 3.0 [44]. Both the HTS (Fe–Cr oxides) and LTS ($CuO–ZnO–Al_2O_3$) catalysts were commercial samples from Sud-Chemie (India) operated under conditions recommended by the catalyst manufacturer. With this realistic feed, $CuO–CeO_2–ZrO_2$ exhibited higher PROX *selectivity* than $CuO–CeO_2$ and $CuO–ZrO_2$. Long-term experiments with this feed (27 h) also confirmed the stability of this catalyst even in the presence of realistic amounts of CO_2 and H_2O. The CO content in the effluent from the PROX reactor was consistently below 10 ppm for $CuO–CeO_2$ and 50 ppm for $CuO–CeO_2–ZrO_2$.

Both the PROX activity and selectivity of the CuO are significantly affected by interactions with the underlying support. Bera et al. [45] attributed the promoting effect of CeO_2 in the $CuO–CeO_2–ZrO_2$ system for CO oxidation to the lowering of the redox potentials of the Cu^{2+}/Cu^{1+} and Cu^{1+}/Cu^0 couples in a CeO_2 matrix in relation to CuO and $CuO–ZrO_2$. In agreement with our results (TPR and EPR) they also observed that the Cu species in a $CuO–CeO_2$ matrix require less energy to be reduced and reoxidized than in the case of pure CuO and $CuO–ZrO_2$. The oxidation of CO on metals is known to obey a single site Langmuir–Hinshelwood kinetic model [46] where CO and O_2 compete for the same sites. In the case of a metal–reducible oxide system (like our reduced $Cu–CeO_2–ZrO_2$), we may expect that while CO may adsorb on copper sites, O_2 (and H_2 and H_2O) may adsorb on both the metal (Cu) and support ($CeO_2–ZrO_2$) (Fig. 8). The availability of additional surface oxygen

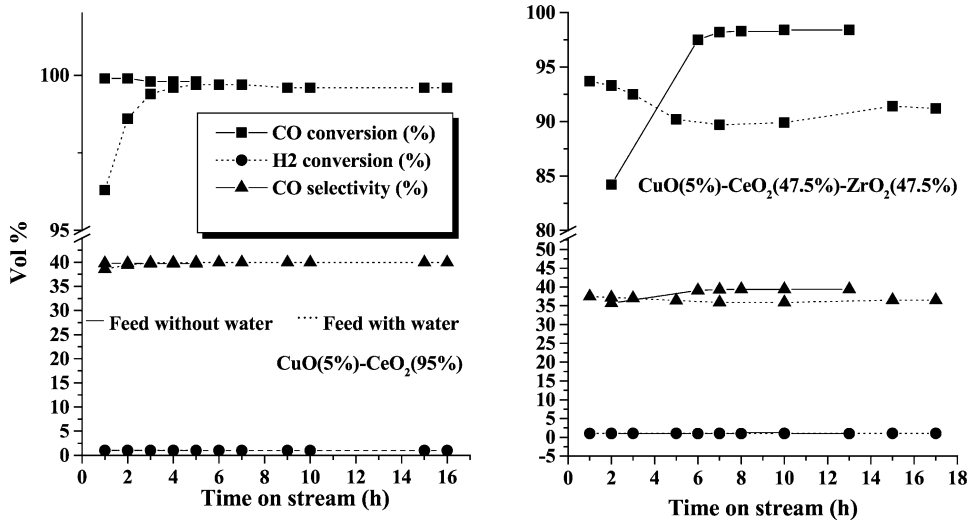

Fig. 9. Influence of time on stream and water in feed on CO and H_2 conversions and CO selectivity. Reaction conditions: catalyst = 1.5 g; feed (H_2 (74.17%) + CO (0.49%) + CO_2 (23.26%) + CH_4 (2.08 v%)) + water ($p(H_2O) = 200$ Torr); $O_2/CO = 1.25$; GHSV = 5000 h^{-1}: catalyst: CuO (5%)–CeO_2 (95%) (left panel); CuO (5%)–CeO_2 (47.5%)–ZrO_2 (47.5%) (right panel).

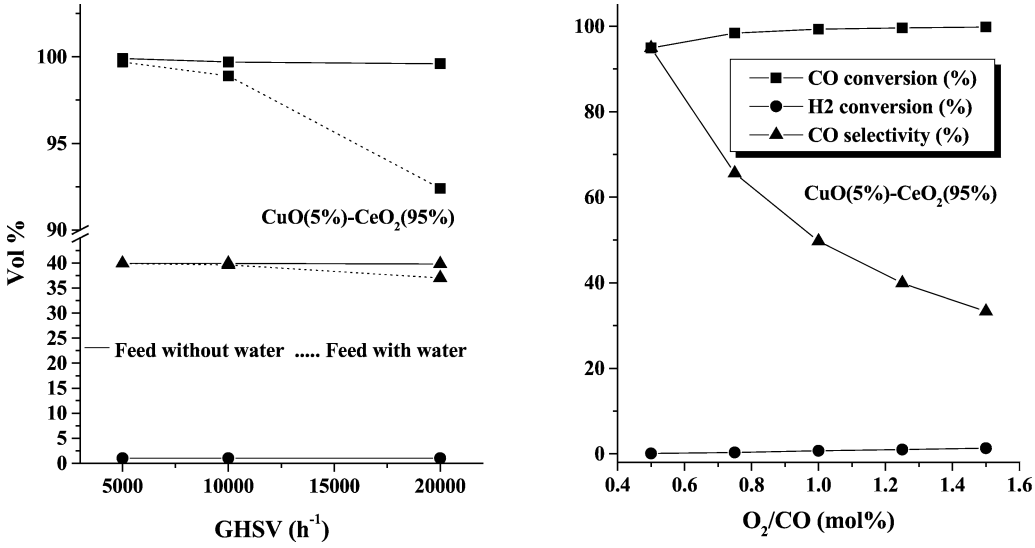

Fig. 10. Effect of space velocity (GHSV; left panel) and O_2/CO (right panel) on the PROX activity/selectivity. Reaction conditions: catalyst (CuO (5%)–CeO_2 (95%) = 1.5 g; feed (H_2 (74.17%) + CO (0.49%) + CO_2 (23.26%) + CH_4 (2.08 v%)) + water ($p(H_2O) = 200$ Torr); run time = 4 h.

and the consequent higher activity of CuO–CeO_2 and CuO–CeO_2–ZrO_2 in CO oxidation are, thus, understandable.

Both the XRD and magnetic susceptibility data indicate that the dispersion of supported CuO decreases in the series CeO_2–ZrO_2 > CeO_2 > ZrO_2. EPR and magnetic susceptibility data indicate that while a small amount of copper is incorporated in the CeO_2/ZrO_2, fluorite lattice (forming a solid solution), most of it is present on the surface as isolated, monomeric copper as well as dimeric copper oxo species containing magnetically interacting copper ions, nano-sized copper oxide clusters, and a bulk, CuO-like phase. While the isolated and dispersed CuO species exhibit reversible reduction-oxidation behavior, the bulk CuO-like phase exhibits irreversible reduction behavior. The amount of reducible and reoxidizable CuO content is more on CeO_2 (39.7%) than on CeO_2–ZrO_2 catalysts (31.4%) (EPR). The concentration of the bulk-like CuO phase decreases in the series ZrO_2 > CeO_2 > CeO_2–ZrO_2. The PROX *selectivity* of these samples correlated with the concentration of the *dispersed* nano-sized CuO species.

4. Summary and conclusions

In this study, the influence of composition and preparation procedure in the CeO_2–ZrO_2 system on the structure, reduction behavior, and catalytic activity of supported CuO in the preferential oxidation of CO in the presence of excess H_2 was investigated. The CO oxidation activity/selectivity of CuO on different supports increases in the order CuO–

ZrO_2 < CuO–CeO_2–ZrO_2 ⩽ CuO–CeO_2. A catalyst of composition containing 5% CuO exhibited stable activity in long-term experiments, using as feed the effluent from an actual steam reformer-cum-water–gas-shift reactor combination generating hydrogen from commercial liquefied petroleum gas. The adverse influence of H_2O was accentuated in catalysts containing ZrO_2. Below 423 K and over CuO–CeO_2 with less than 5 wt% CuO, the presence of H_2O in the feed suppressed CO oxidation. The high dispersion and facile reducibility of CuO on CeO_2 and CeO_2–ZrO_2 supports are responsible for their superior activity/selectivity over CuO–ZrO_2 catalysts.

References

[1] D.L. Trimm, Z. Ilsen Önsan, Catal. Rev. Sci. Tech. 43 (2001) 31.
[2] T.V. Choudhary, D.W. Goodman, Catal. Today 77 (2002) 65.
[3] J.R. Rostrup-Nielson, T. Rostrup-Nielson, Cattech 6 (2002) 150.
[4] M.J. Kahlich, H.A. Gasteiger, R.J. Behm, J. Catal. 171 (1997) 93.
[5] H. Igarashi, H. Uchida, M. Suzuki, Y. Sasaki, M. Watanabe, Appl. Catal. A 159 (1997) 159.
[6] S.-I. Ito, T. Fujimori, K. Nagashima, K. Yuzaki, K. Kunimori, Catal. Today 57 (2000) 247.
[7] W.H. Cheng, React. Kinet. Catal. Lett. 58 (1996) 329.
[8] R.M. Torres, A. Sanchez, K. Ueda, K. Tanaka, M. Haruta, J. Catal. 168 (1997) 125.
[9] Y. Teng, H. Sakurai, A. Ueda, T. Kobayashi, Int. J. Hydrogen Energy 24 (1999) 355.
[10] G. Avgouropoulos, T. Ioannides, H.K. Matralis, J. Batista, S. Hocevar, Catal. Lett. 73 (2001) 33.
[11] W. Liu, M. Flytzani-Stephanopoulos, J. Catal. 153 (1995) 304.
[12] M. Haruta, Cattech 6 (2002) 102.
[13] M.J. Kahlich, H.A. Gasteiger, R.J. Behm, J. Catal. 182 (1999) 430.
[14] G. Avgouropoulos, T. Ioannides, Ch. Papadopoulou, J. Batista, S. Hocevar, H.K. Matralis, Catal. Today 75 (2002) 157.
[15] G.K. Bethke, H.H. Kung, Appl. Catal. A 194–195 (2000) 43.
[16] R.J.H. Grisel, B.E. Nieuwenhuys, J. Catal. 199 (2001) 48.
[17] M.M. Schubert, V. Plzak, J. Garche, R.J. Behm, Catal. Lett. 76 (2001) 143.
[18] Y.-F. Han, M.J. Kahlich, M. Kinne, R.J. Behm, Phys. Chem. Chem. Phys. 4 (2002) 389.
[19] S.-M. Zhang, W.-P. Huang, X.-H. Qiu, B.-Q. Li, X.-C. Zheng, S.-H. Wu, Catal. Lett. 80 (2002) 41.
[20] D.H. Kim, M.S. Lim, Appl. Catal. A 224 (2002) 27.
[21] O. Korotkikh, R. Farrauto, Catal. Today 62 (2000) 249.
[22] J.B. Wang, W.H. Shih, T.-J. Huang, Appl. Catal. A 203 (2000) 191.
[23] H. Vidal, J. Kašpar, M. Pijolat, G. Colon, S. Bernal, A. Cordón, V. Perrichon, F. Fally, Appl. Catal. B 27 (2000) 49.
[24] A. Martínez-Arias, M. Fernández-García, J. Soria, J.C. Conesa, J. Catal. 182 (1999) 367.
[25] A. Martínez-Arias, M. Fernández-García, O. Gálvez, J.M. Coronado, J.A. Anderson, J.C. Conesa, J. Soria, G. Munuera, J. Catal. 195 (2000) 207.
[26] A. Martínez-Arias, M. Fernández-García, A.B. Hungría, A. Iglesias-Juez, O. Gálvez, J.A. Anderson, J.C. Conesa, J. Soria, G. Munuera, J. Catal. 214 (2003) 261.
[27] J. Xiaoyuan, L. Guanglie, Z. Renxian, M. Jianxin, C. Yu, Z. Xiaoming, Appl. Surf. Sci. 173 (2001) 208.
[28] M.-F. Luo, Y.-J. Zhong, X.-X. Yuan, X.-M. Zheng, Appl. Catal. A 162 (1997) 121.
[29] G. Avgouropoulos, T. Ioannides, Appl. Catal. A 244 (2003) 155.
[30] H. Tanaka, S.-I. Ito, S. Kameoka, K. Tomishige, K. Kunimori, Catal. Commun. 4 (2003) 1.
[31] A. Martínez-Arias, M. Fernández-García, V. Ballesteros, L.N. Salamanca, J.C. Conesa, C. Otero, J. Soria, Langmuir 15 (1999) 4796.
[32] W. Liu, M. Flytzani-Stephanopoulos, Chem. Eng. J. 64 (1996) 283.
[33] L. Kundakovic, M. Flytzani-Stephanopoulos, Appl. Catal. A 171 (1998) 13.
[34] G. Wrobel, C. Lamonier, A. Bennani, A. D'Huysser, A. Aboukais, J. Chem. Soc., Faraday Trans. 92 (1996) 2001.
[35] A. Bensalem, F. Bozon-Verduraz, M. Delamar, G. Bugli, Appl. Catal. A 121 (1995) 81.
[36] H. Praliaud, S. Mikhailenko, Z. Chajar, M. Primet, Appl. Catal. B 16 (1998) 359.
[37] S. Velu, K. Suzuki, M. Okazaki, M.P. Kapoor, T. Osaki, F. Ohashi, J. Catal. 194 (2000) 373.
[38] P.I. Paulose, G. Jose, V. Thomas, G. Jose, N.V. Unnikrishnan, M.K.R. Warrier, Bull. Mater. Sci. 25 (2002) 69.
[39] J.L.G. Fierro, J. Soria, J. Sanz, J.M. Rojo, J. Solid State Chem. 66 (1987) 154.
[40] M. Che, J.F.J. Kibblewhite, A.J. Tench, M. Dufaux, C. Naccache, J. Chem. Soc., Faraday Trans. I 69 (1973) 857.
[41] P.G. Harrison, I.K. Ball, W. Azelee, W. Daniell, D. Goldfarb, Chem. Mater. 12 (2000) 3715.
[42] A. Aboukais, A. Bennani, C.F. Aïssi, G. Wrobel, M. Guelton, J.C. Vedrine, J. Chem. Soc., Faraday Trans. 88 (1992) 615.
[43] M.M. Gunter, T. Ressler, R.E. Jentoft, B. Bems, J. Catal. 203 (2001) 133.
[44] P. Ratnasamy, D. Srinivas, H.S. Soni, A.J. Chandwadkar, H.S. Potdar, C.S. Gopinathand, B.S. Rao, Stud. Surf. Sci. Catal. 135 (2001) 1270.
[45] P. Bera, S. Mitra, S. Sampath, M.S. Hegde, Chem. Commun. (2001) 927.
[46] R.J. Farrauto, C. Bartholomew, Introduction to Industrial Catalytic Processes, Chapman & Hall, London, 1997, Chaps. 1, 38, 39.